The Astrophysical Journal Letters, 837:L11 (7pp), 2017 March 1 https://doi.org/10.3847/2041-8213/aa611b

Determination of the Alfvén Speed and Plasma-beta Using the Seismology of Sunspot Umbra

I.-H. Cho[1], K.-S. Cho[2,3], S.-C. Bong[2,3], Y.-J. Moon[1,4], V. M. Nakariakov[1,5], J. Park[1,2], J.-H. Baek[2], S. Choi[1,2], Y.-H. Kim[2,3], and J. Lee[2,3]
[1] Department of Astronomy and Space Science, Kyung Hee University, Yongin 446-701, Korea; ihjo@khu.ac.kr
[2] Space Science Division, Korea Astronomy and Space Science Institute, Daejeon 305-348, Korea
[3] Department of Astronomy and Space Science, University of Science and Technology, Daejeon 305-348, Korea
[4] School of Space Research, Kyung Hee University, Yongin 446-701, Korea
[5] Centre for Fusion, Space and Astrophysics, Physics Department, University of Warwick, Coventry CV4 7AL, UK
Received 2016 November 30; revised 2017 January 29; accepted 2017 February 6; published 2017 March 2

Abstract

For 478 centrally located sunspots observed in the optical continuum with *Solar Dynamics Observatory*/Helioseismic Magnetic Imager, we perform seismological diagnostics of the physical parameters of umbral photospheres. The new technique is based on the theory of slow magnetoacoustic waves in a non-isothermally stratified photosphere with a uniform vertical magnetic field. We construct a map of the weighted frequency of three-minute oscillations inside the umbra and use it for the estimation of the Alfvén speed, plasma-beta, and mass density within the umbra. We find the umbral mean Alfvén speed ranges between 10.5 and 7.5 km s^{-1} and is negatively correlated with magnetic field strength. The umbral mean plasma-beta is found to range approximately between 0.65 and 1.15 and does not vary significantly from pores to mature sunspots. The mean density ranges between (1–6) $\times$ 10^{-4} kg m^{-3} and shows a strong positive correlation with magnetic field strength.

Key words: methods: data analysis – Sun: oscillations – Sun: photosphere – sunspots

Supporting material: data behind figure, machine-readable table

1. Introduction

A sunspot is a localized region of the density depletion relative to the surrounding plasma due to the magnetic pressure (Low 1992), which leads to the increased transparency in the optical band (Jensen et al. 1969). Thus the emission associated with a certain spectral line in the sunspot may be mostly contributed from below the line forming height in the quiet region. Depending on the sunspot magnetic field strength, the line forming height could be depressed up to several hundred kilometers (Solanki et al. 1993; Moon et al. 1998; Mathew et al. 2004). This is the so-called Wilson effect (Wilson & Maskelyne 1774). As the density of the umbra increases as the height decreases (Maltby et al. 1986), similarly to the quiet Sun (Fontenla et al. 2007), the density measured from a certain spectral line may be positively dependent on the magnetic field strength.

Physical parameters of the umbra are important for our understanding of the formation and evolution of a sunspot. Photospheric temperatures inside an umbra can be measured directly from the continuum ratio relative to the quiet Sun (Solanki et al. 1993; Jaeggli et al. 2012). Observations of other important parameters, such as the density and gas pressure in the umbra, is more difficult, as it requires a careful consideration of the line forming and reference heights (Khomenko & Collados 2015).

The combination of the theory of magnetohydrodynamic (MHD) waves with observations of solar atmospheric waves and oscillations gives information on the physical parameters of medium (e.g., Nakariakov et al. 2016), including sunspots (e.g., see Snow et al. 2015; Sych 2016 for recent results). Moreels & van Doorsselaere (2013) designed a method for deriving the temperature of plasma confined in photospheric magnetic flux tubes by using the intensity, velocity, and magnetic field strength fluctuation amplitudes. Reznikova et al. (2012) estimated the inclination angle of umbral magnetic field, based on the interpretation of umbral oscillation as a slow magnetoacoustic gravity (MAG) wave in an inclined magnetic field. Yuan et al. (2014) established that the magnetic inclination angle derived seismologically was 30%–40% larger than that given by the magnetic field extrapolation. Roberts (2004) reviewed the analytical expressions for the cutoff frequency as a function of observable parameters for different solar atmospheric models.

Roberts (2006) provided an analytical form of angular cutoff frequency of a slow magnetoacoustic wave in a non-isothermally stratified atmosphere with a uniform vertical magnetic field. The cutoff frequency not only prescribes the lowest frequency of a propagating wave, but also acts as a natural frequency of a medium (e.g., Roberts 2004). It suggests that the atmosphere should be observed to oscillate at the frequency equal or higher than the cutoff frequency in response to an external broadband excitation (Botha et al. 2011; Chae & Goode 2015; Kwak et al. 2016). Thus, the cutoff frequency is always below the detected frequency (e.g., Tziotziou et al. 2006; Yuan et al. 2014). Thus, the cutoff frequency involves the physical parameter of the medium, independently of the specific excitation mechanism of atmospheric oscillations.

In this work, we determine the cutoff frequency of umbral oscillations by using the weighted frequency, $\langle f \rangle = \sum P(f) f / \sum P(f)$, where $P(f)$ is the power spectrum (Takahashi et al. 2015), for 478 sunspots observed in the continuum with the Heliospheric Magnetic Imager (HMI; Scherrer et al. 2012; Schou et al. 2012) on board the *Solar Dynamics Observatory* (*SDO*; Pesnell et al. 2012). Using the theory given by Roberts (2006), we determine the Alfvén speed, plasma-beta (β), and mass density inside umbrae. In Section 2, we describe the method used to obtain the weighted frequency and its link with the Alfvén speed, plasma-β, and mass density. In Section 3, we

provide maps of those quantities as well as their average behavior for the 478 analyzed sunspots. Finally, we summarize and discuss our results.

2. Method: Seismology

We derive the physical parameters of an umbra by using the seismology, developing the approach designed by Yuan et al. (2014), who estimated acoustic cutoff frequencies of umbral oscillations at the heights of 1700, 1600, and 304 Å line formation. The authors found that the acoustic cutoff frequency is linearly scaled with the observed peak frequency ($f_{\rm cutoff} = a f_{\rm peak} + b$), with the scaling factor $a \approx 0.65$ and ordinate $b \approx 0.57$ mHz. Accepting this finding, we assume that the cutoff frequency could be determined from the peak frequencies.

The power spectra of umbral oscillations often have multiple peaks around 5 mHz. Taking the frequency with the highest power only does not account for this feature. Therefore, we use the weighted frequency, summed up in the frequency range from 0 to the Nyquist frequency. As shown in Figure 1(b), the weighted frequency is close to the peak frequency.

The three-minute oscillation can be modulated by lower-frequency variations (e.g., Sych et al. 2012; Chae & Goode 2015), which is hard to remove in the 1st derivative. To reduce a possible contribution of low-frequency powers to the weighted frequency, we take the 2nd time derivative of a 1 hr time series of the HMI continuum. Then we subtract a trend given by straight-line fitting. The residual time series are enlarged to 512 points by adding zero signals to increase the frequency sampling in the spectrum.

Rae & Roberts (1982) derived the dispersion relation for slow magnetoacoustic waves in a vertical thin magnetic flux tube in a non-isothermally stratified atmosphere, which involves scale heights of various physical quantities. Here, we consider a uniform magnetic field to describe the photospheric umbra. In the finite-β plasma, the phase speed of these waves is determined by the combination of local sound speed and Alfvén speed. The analytical form of the angular cutoff frequency of slow magnetoacoustic waves is given by the following expression (Roberts 2006):

$$\Omega^2 = c_{\rm T}^2 \left\{ \frac{1}{4\Lambda_p^2}\left(\frac{c_{\rm T}}{c_{\rm S}}\right)^4 - \frac{\gamma g}{2}\left(\frac{c_{\rm T}^2}{c_{\rm S}^4}\right)' + \frac{1}{c_{\rm A}^2}\left(\omega_g^2 + \frac{g}{\Lambda_p}\frac{c_{\rm T}^2}{c_{\rm S}^2}\right)\right\}, \quad (1)$$

where $\Omega = 2\pi f_{\rm cutoff}$ and $f_{\rm cutoff}$ is the cutoff frequency to be determined by scaling the weighted frequency. The quantities $c_{\rm S}$ $(=\sqrt{\gamma m_{\rm H} T_0/(\mu m_{\rm H})})$, $c_{\rm A}$ $(=B_0/\sqrt{\mu_{\rm B}\rho_0})$, and $c_{\rm T}$ $(=c_{\rm S}c_{\rm A}/\sqrt{c_{\rm S}^2 + c_{\rm T}^2})$ are the sound speed, Alfvén speed, and tube speed, respectively, and γ, $k_{\rm B}$, T_0, μ, $m_{\rm H}$, B_0, $\mu_{\rm B}$, and ρ_0 are the specific heat ratio, Boltzmann's constant, temperature, mean molecular weight, hydrogen atomic mass, magnetic field strength, magnetic permeability, and density, respectively. The subscript 0 indicates the equilibrium quantity. The ω_g^2 $(=g/\Lambda_\rho - g^2/c_{\rm A}^2)$ is the buoyancy frequency, where $g = 0.274$ km s^{-2}. The parameters Λ_p $(=c_{\rm S}^2/(\gamma g))$ and Λ_ρ $(=-\rho_0/\rho_0')$ are the pressure and density scale heights, respectively. The prime indicates the derivative with respect to the vertical direction. As we assume the uniform vertical field in a non-isothermal stratified medium, $(c_{\rm A}^2)' = c_{\rm A}^2(z)/\Lambda_\rho$ and $(c_{\rm S}^2)' = c_{\rm S}^2(z)/\Lambda_\rho - \gamma g$, giving $(c_{\rm T}^2)' = c_{\rm T}^2/\Lambda_\rho - \gamma g c_{\rm T}^4/c_{\rm S}^4$. Hence the expression for the angular cutoff frequency is reduced to

$$\Omega^2 = \frac{3\gamma g}{4\Lambda_p}X^3 + \left(\frac{\gamma g}{2\Lambda_\rho} - \frac{\gamma g}{\Lambda_p} - \frac{g}{\Lambda_p}\right)X^2 + \left(\frac{g}{\Lambda_p} - \frac{g}{\Lambda_\rho} + \frac{g}{\gamma\Lambda_p}\right)X + \frac{g}{\Lambda_\rho} - \frac{g}{\gamma\Lambda_p}, \quad (2)$$

where $X \equiv c_{\rm T}^2/c_{\rm S}^2$. Equation (2) describes umbral oscillations in the photosphere, accounting for the finite β effects. Equation (2) shows that $f_{\rm cutoff}$ is directly related to Λ_p and Λ_ρ, which all can be determined from observations. In other words, $\Lambda_p = c_{\rm S}^2/(\gamma g)$ and $\Lambda_\rho = \gamma\Lambda_p$. Thus, Equation (2) becomes a function of X.

The sound speed $c_{\rm S}$ is estimated from the plasma temperature. The temperature is obtained from the ratio of HMI continuum intensity to the quiet Sun's, by applying the Planck function (Mathew et al. 2004). In other words, we solve the equation $I\,(e^{hc/\lambda k_{\rm B} T_{U,0}} - 1) = e^{hc/\lambda k_{\rm B} T_{Q,0}} - 1$, where I, h, c, λ, $k_{\rm B}$, $T_{U,0}$, and $T_{Q,0}$ are the intensity ratio, Planck's constant, speed of light, wavelength of Fe I line continuum (6172.1 Å), Boltzmann's constant, the temperature at a given position, and the temperature of the quiet Sun (6000 K), respectively. Using $\mu = 1.3$ and $\gamma = 5/3$, we obtain the sound speed as $103.26\sqrt{T\,(MK)}$ km s^{-1}.

We look for a positive solution for X of Equation (2) by changing the scaling of $f_{\rm cutoff}/\langle f\rangle$ in the range below 1.0. We found that positive solutions for all pixels inside the umbra exist when the scaling is in 0.5–0.55. Thus we take 0.55 as the upper limit of the scaling.

The solution $X = c_{\rm T}^2/c_{\rm S}^2$ allows us to calculate the Alfvén speed, using the expressions $c_{\rm A} = c_{\rm S}c_{\rm T}/\sqrt{c_{\rm S}^2 - c_{\rm T}^2}$), the plasma-$\beta$, as $\beta = 2c_{\rm S}^2/(\gamma c_{\rm A}^2)$, and the mass density as $\rho_0 = B_0^2/(\mu_{\rm B} c_{\rm A}^2)$ for each pixel of the umbra. The magnetic field strength B_0 is obtained as the de-projected HMI magnetogram, which may correspond to the magnetic field slightly above the height of continuum formation (Norton et al. 2006). Slightly different values of equilibrium quantities do not give us significantly different results. For example, when $\delta T_0 = \pm 100$ K, $|\delta c_{\rm S}|$ and $|\delta c_{\rm A}|$ are less than 50 m s^{-1}, and $|\delta\beta|$ is less than 0.02 for the given sunspot. When we choose $\delta\lambda = -2$ Å, the absolute values of deviation of speeds and plasma-β are less than 0.1 m s^{-1} and 10^{-4}, respectively.

3. Results

We illustrate the application of the developed method to a sunspot located near the disk center, observed during 00:00–01:00 UT on 2014 August 28, in NOAA 12149. The center of a sunspot is tracked synodically, accounting for the effect of the solar differential rotation. We used the differential rotation law, $\omega(\varphi) = 2.894 - 0.428\sin^2(\varphi) - 0.370\sin^4(\varphi)$ in μrad s^{-1}, where φ is the latitude (Howard et al. 1990). We uniformly interpolate the region occupied by $\pm 4°$ in heliographic longitude and latitude (Thompson 2006) from the sunspot center with a fixed binsize of 0°.04. Figure 1(a) shows an HMI continuum image of the sunspot in heliographic coordinate. The white contour indicates the umbral boundary obtained by the two-step intensity thresholding technique (Cho

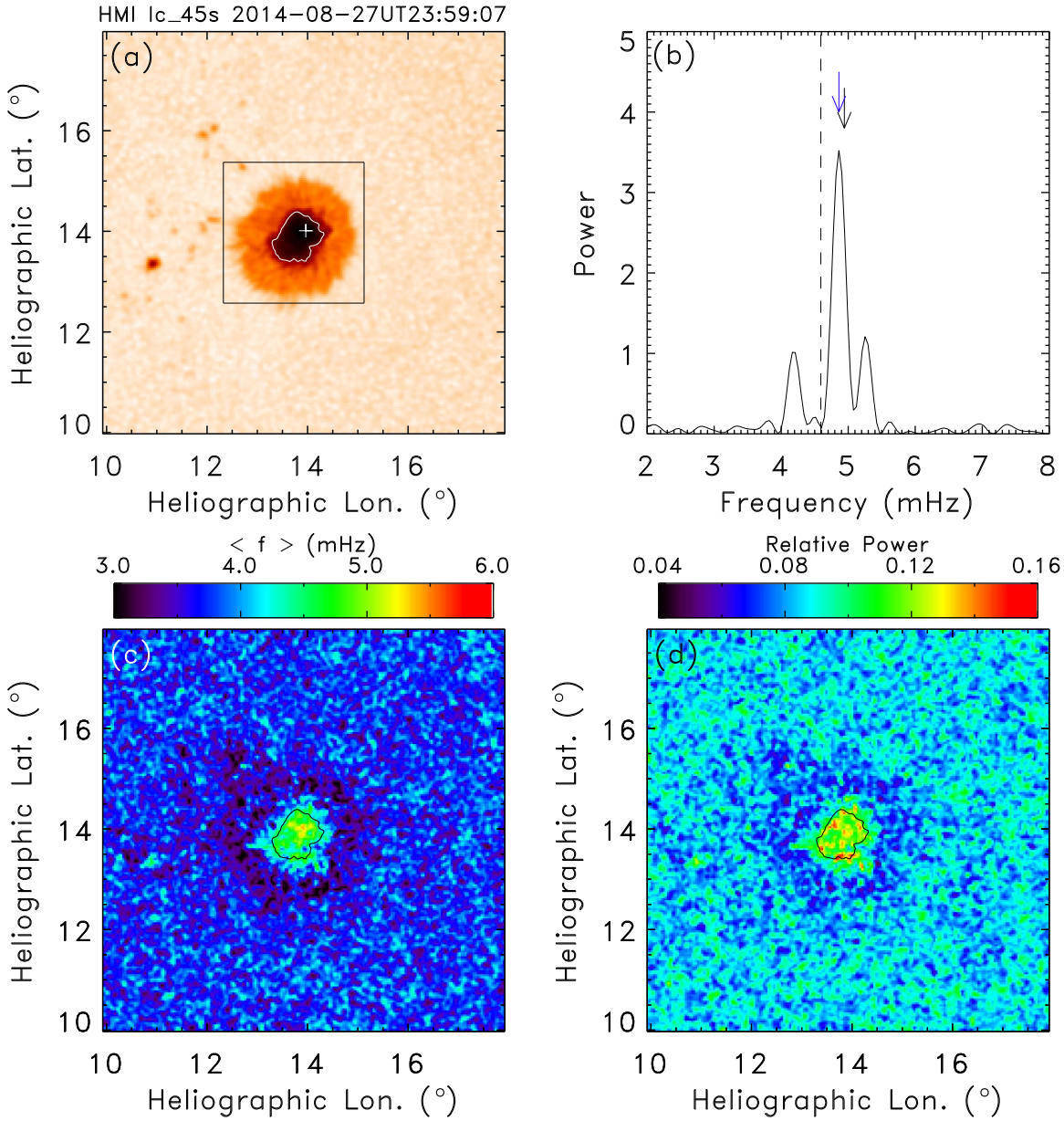

Figure 1. Panel (a): the map of HMI continuum of an analyzed sunspot, the white contour indicates the umbral boundary; (b) example of a power spectrum; (c) the map of the weighted frequency; (d) and corresponding power. The rectangular box in (a) is the region used in Figures 2 and 3. The white cross is the position used to obtain the example of power spectrum. The blue and black arrows in panel (b) indicate the peak frequency and $\langle f \rangle$, respectively. The vertical dashed line represents $\langle f \rangle - \sigma_f/4$. The contour inside the sunspot is the umbral boundary.

et al. 2015). Figure 1(b) shows an example of the power spectrum at the position indicated by the white cross in panel (a). Figure 1(c) shows the spatial distribution of weighted frequency. It is evident that the oscillation in the frequency range 4–5 mHz is pronounced inside the umbra. The corresponding power is also prominent inside the umbra (Figure 1(d)). The power is defined by averaging the power spectrum in the frequency range from $\langle f \rangle - \sigma_f/4$ to $f_{\rm Nyquist}$ to exclude the possible contribution of five-minute oscillations. The value σ_f is defined as $\sigma_f^2 = \sum P(f)(f - \langle f \rangle)^2 / \sum P(f)$. The time series at each pixel was normalized by its standard deviation before the Fourier transform.

From the map of the weighted frequency for the box indicated in Figure 1(a), we construct the map of $c_{\rm T}$ by applying the method described in Section 2. We use the scaling relation $f_{\rm cutoff} = 0.55 \langle f \rangle$ and $\Lambda_\rho = \gamma \Lambda_p$ to solve Equation (2) for each pixel. Thus, we obtain the spatial distribution of the Alfvén speed and then plasma-β and mass density (Figure 2). Figures 2(d)–(f) show the dependence of these parameters on the magnetic field strength inside the umbra. It is found that the Alfvén speed and plasma-β inside the umbra do not show any correlation with the field strength. The Alfvén speed ranges from 5–14 km s^{-1}, mainly 6–11 km s^{-1}. The plasma-β is established to be 0.3–1.6. The density inside the umbral photosphere ranges from (1–10) $\times$ 10^{-4} kg m^{-3}, which gives the number density $\sim$10^{16}–10^{17} cm^{-3}. These values are comparable with the typical photospheric values (e.g., Zirin 1988, p.138). The density inside the umbra is highly dependent (the correlation coefficient, CC = 0.82) on the field strength. The density seems to have higher values in the central

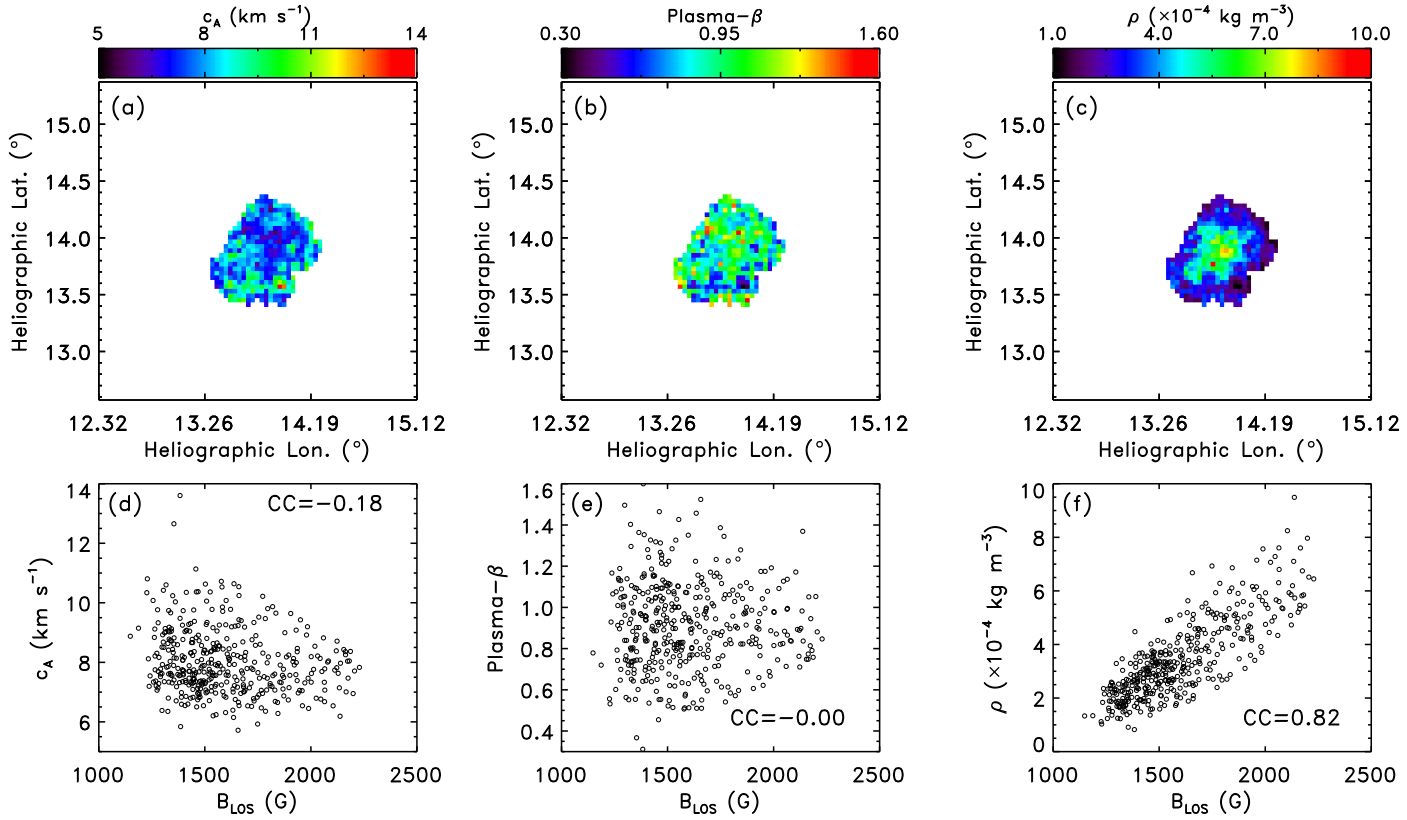

Figure 2. Spatial distribution of the Alfvén speed (a), plasma-β (b), and mass density (c) of the umbra shown in Figure 1 with their dependency on the magnetic field strength (d)–(f) inside the umbra. The CC represents the correlation coefficient.

part of the umbra, which may reflect a significant depression of the continuum formation height.

We applied this technique to the analysis of umbral oscillations in 478 sunspots observed during 2012–2015. We selected sunspots located near the disk center ($r/R_\odot < 0.3$, where r and $R_\odot$ are the distances of the umbra from the center of solar disk and the solar radius, respectively). We superpose the umbral boundary on the map of the Alfvén speed, sound speed, plasma-β, and mass density to obtain their mean values. The results are given in Figure 3. Observation times and locations, including average parameters of analyzed sunspots are listed in Table 1.

The blue, green, and red colors represent the pores (<20 MSH), transitional (20–100 MSH), and mature sunspots (>100 MSH), respectively (Tlatov & Pevtsov 2014; Cho et al. 2015). We calculate CC between the mean determined physical parameters of the umbral photosphere and the magnetic field separately for each group. Except for the mean plasma-β, the CC of umbral parameters with the mean magnetic field strength seems to eventually increase from pores to mature sunspots. For example, the CC between the mean Alfvén speed and mean magnetic field strength shows the lowest value in the pores (−0.24) and the highest values in the mature sunspots (−0.53). The CC shown in black is obtained from the whole samples in each panel. The mean umbral sound speed is found to range from 7.8–6.5 km s^{-1}, decreasing from pores to mature sunspots. The Alfvén speed ranges from 10.5–7.5 km s^{-1}, decreasing from pores to mature sunspots too. The mean umbral plasma-β ranges from 0.65–1.15 and does not show any correlation with the mean magnetic field strength. The mean mass density derived by using the HMI magnetogram ranges from 1–6 $\times$ 10^{-4} kg m^{-3} and correlates positively with the mean magnetic field strength. The mean values of the determined physical parameters are summarized in Table 2.

4. Summary and Discussion

We developed a new seismological technique for the determination of the main physical parameters of sunspot atmospheres observed in the HMI continuum. The technique utilizes the dispersion relation for slow magnetoacoustic waves in a non-isothermally stratified atmosphere with a uniform vertical magnetic field and accounts for the finite plasma-β effects. Using this technique, we determined the spatial distribution of the Alfvén speed, plasma-β, and density in umbral photospheres in 478 sunspots observed during 2012–2015 by analyzing continuum oscillations. As we analyzed the centrally located sunspots only, the assumption of the vertical umbral magnetic field seems to be justified.

The measured plasma-β in the umbral photosphere ranges from 0.65–1.15. The mean umbral plasma-β is found to be independent of the mean magnetic field strength and to be the same in pores and transitional and mature sunspots. The plasma-β measured in this study is consistent with results of previous studies. Mathew et al. (2004) directly measured the gas and magnetic pressures from spectro-polarimetric data and found the plasma-β inside the photospheric umbra mostly ranges in 0.5–1.0. Gary (2001) developed a representative model of the magnetic and gas pressure from the photosphere to corona and found that $\beta = 0.1$–1.0 inside the umbral photosphere. Jess et al. (2013) obtained the photospheric $\beta = 1$ contour at the outer boundary of sunspot penumbra by applying the sunspot model (Maltby et al. 1986). We would like to note

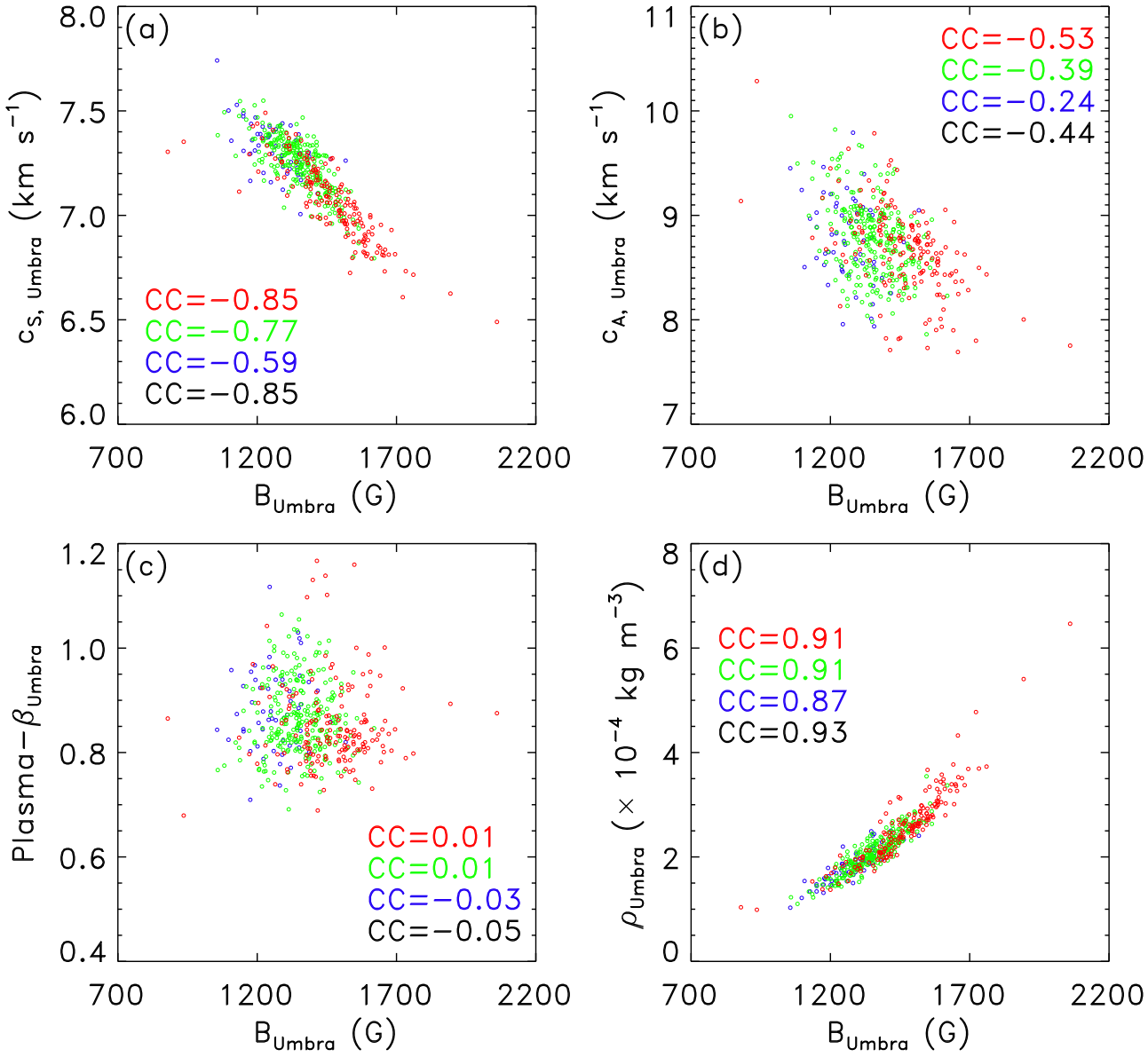

Figure 3. Umbral photospheric mean sound speed (a), Alfvén speed (b), plasma-β (c), and mass density (d) as a function of the mean umbral magnetic field strength. The blue, green, and red circles correspond to the pores, transitional, and mature sunspots. The correlation coefficient (CC) shown in black is calculated from the whole sample. The detailed data set of 478 sunspots is available as data behind the figure.

(The data used to create this figure are available.)

that the measurement of Alfvén speed and plasma-β obtained in our study are determined without knowing the magnetic field strength.

The negative correlation between Alfvén speed and magnetic field strength might be explained by the geometrical effect of the Wilson depression. The mass density of the sunspot plasma rapidly increases as the height decreases (Maltby et al. 1986). Note that the photospheric pressure scale height is approximately 100 km. As the Wilson depression reaches a few hundred kilometers, the density increase is likely to exceeds the enhancement given by the square of the increase in the magnetic field strength, resulting in the reduction of the Alfvén speed, as seen in Figure 3(b). In other words, $\Delta B/B_0 \sim 2$ and $\Delta\rho/\rho_0 \sim 5$ result in $\Delta c_A/c_A \sim 0.8$, which is comparable to 7.5 km s^{-1}/10.5 km s^{-1}. Thus, the physical parameters of the umbral photosphere derived by the seismology with the slow magnetoacoustic wave in the moderate plasma-β are typical.

The developed technique provides us with a tool for the quantitative comparison of different models of sunspot atmospheres, e.g., given in Staude (1981), Lites & Skumanich (1982), and Maltby et al. (1986), which is a necessary ingredient of our understanding of sunspot structure and evolution. The use of the designed seismological technique in combination with high-resolution observations may also give a chance to explore the evolution of smaller objects such as tiny pores (Cho et al. 2010, 2013).

This work is supported by the BK21 plus program through the National Research Foundation (NRF) funded by the Ministry of Education (MOE) of Korea and "Planetary system research for space exploration" from Korea Astronomy and Space Science Institute (KASI). Y.J.M. acknowledges the support from Basic Science Research Program through the NRF funded by MOE of Korea (NRF-2016R1A2B4013131)

Table 1
List of 478 Sunspots

Date	Start Time	X ($''$)	Y ($''$)	$B_{\rm Umbra}$ (G)	Area (MSH)	$\langle f_{\rm Umbra} \rangle$ (mHz)	$c_{\rm S,Umbra}$ (km s^{-1})	$c_{\rm T,Umbra}$ (km s^{-1})	$c_{\rm A,Umbra}$ (km s^{-1})	Plasma $-\beta_{\rm Umbra}$	$\rho_{\rm Umbra}$ ($\times 10^{-4}$ kg m^{-3})
2012 Mar 25	23:59:02	−56.73	−120.77	1292.71 ± 188.27	17.83	4.25 ± 0.35	7.23 ± 0.07	5.59 ± 0.29	8.94 ± 1.22	0.82 ± 0.19	1.84 ± 0.83
2012 Mar 26	23:59:02	167.16	−126.31	1253.19 ± 121.53	13.83	4.29 ± 0.29	7.30 ± 0.09	5.58 ± 0.26	8.72 ± 0.89	0.87 ± 0.17	1.69 ± 0.41
2012 Mar 28	23:59:02	−106.65	−263.97	1417.20 ± 268.41	175.75	4.16 ± 0.38	6.99 ± 0.16	5.59 ± 0.32	9.53 ± 1.59	0.69 ± 0.18	2.01 ± 1.09
2012 Apr 12	23:59:04	50.17	207.50	1192.08 ± 138.42	49.98	4.30 ± 0.27	7.37 ± 0.11	5.59 ± 0.26	8.65 ± 0.86	0.89 ± 0.18	1.59 ± 0.53
2012 May 29	23:59:10	−209.03	−182.80	1383.03 ± 183.95	30.91	4.23 ± 0.28	7.27 ± 0.11	5.63 ± 0.24	8.96 ± 0.92	0.82 ± 0.17	2.01 ± 0.75
2012 May 29	23:59:10	176.75	−208.52	1341.84 ± 207.11	71.06	4.27 ± 0.28	7.17 ± 0.10	5.56 ± 0.24	8.89 ± 1.03	0.81 ± 0.16	1.95 ± 0.82
2012 May 29	23:59:10	192.89	−146.49	1126.89 ± 116.87	16.89	4.17 ± 0.28	7.53 ± 0.04	5.74 ± 0.25	8.97 ± 1.03	0.87 ± 0.17	1.34 ± 0.46
2012 May 29	23:59:10	206.50	−171.71	1252.38 ± 184.96	30.72	4.21 ± 0.29	7.35 ± 0.09	5.66 ± 0.26	8.97 ± 1.00	0.84 ± 0.20	1.66 ± 0.68
2012 May 29	23:59:10	80.43	−214.07	1413.52 ± 206.63	51.70	4.41 ± 0.31	7.18 ± 0.12	5.44 ± 0.27	8.44 ± 0.96	0.90 ± 0.20	2.39 ± 0.98
2012 Jun 04	23:59:10	−66.82	250.88	1563.79 ± 202.23	92.00	4.45 ± 0.37	6.87 ± 0.16	5.34 ± 0.31	8.57 ± 1.05	0.80 ± 0.21	2.87 ± 1.29
2012 Jul 28	23:59:10	48.16	195.92	1377.13 ± 176.21	34.02	4.29 ± 0.30	7.28 ± 0.11	5.57 ± 0.27	8.74 ± 0.94	0.86 ± 0.19	2.10 ± 0.79
2012 Sep 09	23:59:05	−13.87	260.96	1426.59 ± 176.55	67.31	4.28 ± 0.29	7.16 ± 0.11	5.55 ± 0.24	8.86 ± 0.90	0.81 ± 0.16	2.17 ± 0.73
2012 Sep 23	23:59:04	−116.74	15.38	1374.67 ± 212.25	184.64	4.30 ± 0.36	7.14 ± 0.21	5.52 ± 0.32	8.85 ± 1.18	0.82 ± 0.22	2.09 ± 0.98
2012 Sep 24	23:59:03	−208.52	25.47	1380.40 ± 127.76	28.59	4.42 ± 0.31	7.38 ± 0.08	5.46 ± 0.33	8.22 ± 1.04	1.02 ± 0.33	2.39 ± 0.81
2012 Sep 24	23:59:03	108.17	12.86	1389.90 ± 226.83	180.20	4.41 ± 0.35	7.07 ± 0.19	5.42 ± 0.30	8.54 ± 1.07	0.86 ± 0.20	2.31 ± 1.12

(This table is available in its entirety in machine-readable form.)

Table 2
Average Values of the Physical Parameters of Umbra in Three Groups of Solar Surface Magnetic Structures

Group	Sound Speed (km s^{-1})	Alfvén Speed (km s^{-1})	Plasma-β	Mass Density ($\times 10^{-4}$ kg m^{-3})
Pores	7.39 ± 0.14	8.73 ± 0.37	0.86 ± 0.07	1.67 ± 0.34
Transitional Sunspots	7.29 ± 0.12	8.73 ± 0.33	0.85 ± 0.06	1.94 ± 0.36
Mature Sunspots	7.14 ± 0.17	8.63 ± 0.38	0.83 ± 0.06	2.21 ± 0.58

and NRF of Korea Grant funded by the Korean Government (NRF-2013M1A3A3A02042232). The *SDO* data were (partly) provided by the Korean Data Center (KDC) for *SDO* in cooperation with NASA and the *SDO*/HMI Team. V.M.N. acknowledges support from the European Research Council under the *SeismoSun* Research Project No. 321141.

References

Botha, G. J. J., Arber, T. D., Nakariakov, V. M., & Zhugzhda, Y. D. 2011, ApJ, 728, 84
Chae, J., & Goode, P. R. 2015, ApJ, 808, 118
Cho, I.-H., Cho, K.-S., Bong, S.-C., et al. 2015, ApJ, 811, 49
Cho, K.-S., Bong, S.-C., Chae, J., et al. 2013, SoPh, 288, 23
Cho, K.-S., Bong, S.-C., Chae, J., Kim, Y.-H., & Park, Y.-D. 2010, ApJ, 723, 440
Fontenla, J. M., Balasubramaniam, K. S., & Harder, J. 2007, ApJ, 667, 1243
Gary, G. A. 2001, SoPh, 203, 71
Howard, R. F., Harvey, J. W., & Forgach, S. 1990, SoPh, 130, 295
Jaeggli, S. A., Lin, H., & Uitenbroek, H. 2012, ApJ, 745, 133
Jensen, E., Brahde, R., & Ofstad, P. 1969, SoPh, 9, 397
Jess, D. B., Reznikova, V. E., van Doorsselaere, T., Keys, P. H., & Mackay, D. H. 2013, ApJ, 779, 168
Khomenko, E., & Collados, M. 2015, LRSP, 12, 6
Kobanov, N. I., Kolobov, D. Y., Chupin, S. A., & Nakariakov, V. M. 2011, A&A, 525, A41
Kwak, H., Chae, J., Song, D., et al. 2016, ApJL, 821, L30
Lites, B. W., & Skumanich, A. 1982, ApJS, 49, 293
Low, B. C. 1992, ApJ, 399, 300
Maltby, P., Avrett, E. H., Carlsson, M., et al. 1986, ApJ, 306, 284
Mathew, S. K., Solanki, S. K., Lagg, A., et al. 2004, A&A, 422, 693
Moon, Y.-J., Yun, H. S., & Park, J.-S. 1998, ApJ, 494, 851
Moreels, M. G., & van Doorsselaere, T. 2013, A&A, 551, A137
Nakariakov, V. M., Pilipenko, V., Heilig, B., et al. 2016, SSRv, 200, 75
Norton, A. A., Graham, J. P., Ulrich, R. K., et al. 2006, SoPh, 239, 69
Pesnell, W. D., Thompson, B. J., & Chamberlin, P. C. 2012, SoPh, 275, 3
Rae, I. C., & Roberts, B. 1982, ApJ, 256, 761
Reznikova, V. E., Shibasaki, K., Sych, R. A., & Nakariakov, V. M. 2012, ApJ, 746, 119
Roberts, B. 2004, Oscillations and Small-Scale Transient Events in the Solar Atmosphere: A Joint View from SOHO and TRACE, Proceedings of SOHO 13—Waves (ESA SP-547; Noordwijk: ESA), 1
Roberts, B. 2006, RSPTA, 364, 447
Scherrer, P. H., Schou, J., Bush, R. I., et al. 2012, SoPh, 275, 207
Schou, J., Scherrer, P. H., Bush, R. I., et al. 2012, SoPh, 275, 229
Snow, B., Botha, G. J. J., & Régnier, S. 2015, A&A, 580, A107
Solanki, S. K., Walther, U., & Livingston, W. 1993, A&A, 277, 639
Staude, J. 1981, A&A, 100, 284
Sych, R. 2016, GMS, 216, 467
Sych, R., Zaqarashvili, T. V., Nakariakov, V. M., et al. 2012, A&A, 539, 23
Takahashi, K., Denton, R. E., Kurth, W., et al. 2015, JGR, 120, 526
Thompson, W. T. 2006, A&A, 449, 791
Tlatov, A. G., & Pevtsov, A. A. 2014, SoPh, 289, 1143
Tziotziou, K., Tsiropoula, G., Mein, N., & Mein, P. 2006, A&A, 456, 689
Wilson, A., & Maskelyne, N. 1774, RSPT, 64, 1
Yuan, D., Sych, R., Reznikova, V. E., & Nakariakov, V. M. 2014, A&A, 561, A19
Zirin, H. 1988, Astrophysics of the Sun (Cambridge: Cambridge Univ. Press)